Improving Aerosol Retrieval From MISR With a Physics-Informed Deep Learning Method

Wenjing Man, Minghui Tao, Lina Xu, Xiaoguang Xu, Jianfang Jiang, Jun Wang, *Member, IEEE*, Lunche Wang, Yi Wang, Meng Fan, and Liangfu Chen

Abstract— The Multi-angle Imaging SpectroRadiometer (MISR) measurement with a large range of scattering angles provides valuable information about aerosol microphysical properties. The current MISR algorithm utilizes predefined aerosol mixtures in lookup tables (LUTs) to infer aerosol types and microphysical parameters, which performs well globally but remains subject to considerable uncertainties in regional scales. To make efficient use of MISR measurement, we developed a physics-informed deep learning (PDL) method to retrieve aerosol optical/microphysical parameters over land in eastern China. By combining the physical constraint of radiative transfer (RT) simulation and modeling ability of DL methods, each aerosol parameter can be modeled with the whole used MISR measurements separately with high computational efficiency. PDL aerosol optical depth (AOD) and fine AOD (FAOD) have high correlation coefficients ($R > 0.95$) with AErosol RObotic NETwork (AERONET) observations, with 89% and 81% values falling into expected error (EE) envelope of $\pm (0.05 + 20\% \text{AOD}_{\text{AERONET}})$, respectively. Despite only a slightly higher accuracy than recent MISR Version 23 products, PDL retrievals have solved the underestimation problem of AOD and FAOD at moderate-to-high values (>0.4). Besides better constraint of abnormal values in coarse AOD (CAOD), the PDL algorithm significantly improves the retrieval accuracy of MISR single scattering albedo (SSA). With reliable and robust performance, the PDL algorithm provides a flexible and efficient aerosol retrieval framework for emerging multiangle polarimetric (MAP) measurements.

Index Terms— Aerosol algorithm, deep learning (DL), eastern China, multiangle, Multi-angle Imaging SpectroRadiometer (MISR).

Wenjing Man, Minghui Tao, Jianfang Jiang, Lunche Wang, and Yi Wang are with the Hubei Key Laboratory of Regional Ecology and Environmental Change, School of Geography and Information Engineering, China University of Geosciences, Wuhan 430074, China (e-mail: wjman@cug.edu.cn; taomh@cug.edu.cn; jianfang2020@126.com; wang@cug.edu.cn; wangyi34@cug.edu.cn).

Lina Xu is with Hubei Subsurface Multi-Scale Imaging Key Laboratory, School of Geophysics and Spatial Information, China University of Geosciences, Wuhan 430074, China (e-mail: xulina@cug.edu.cn).

Xiaoguang Xu is with the Department of Physics, GESTAR-II, and the Earth and Space Institute, University of Maryland, Baltimore County, Baltimore, MD 21250 USA (e-mail: xxu@umbc.edu).

Jun Wang is with the Center for Global and Regional Environmental Research, The University of Iowa, Iowa City, IA 52242 USA (e-mail: jun-wang-1@uiowa.edu).

Meng Fan and Liangfu Chen are with the State Key Laboratory of Remote Sensing Science, Aerospace Information Research Institute, Chinese Academy of Sciences, Beijing 100101, China (e-mail: fanmeng@aircas.ac.cn; chenlf@aircas.ac.cn).

Digital Object Identifier 10.1109/TGRS.2024.3376598

I. INTRODUCTION

AS A mixture of solid and liquid particles suspended in the air, atmospheric aerosols have complex physical and chemical properties closely associated with their emission sources. With particle sizes close to the wavelength of sunlight, aerosols scatter and partly absorb incoming solar radiations and alter their distribution in the Earth-atmosphere system [1]. These radiative effects of aerosols, along with their role in cloud condensation nuclei, can modify cloud cover and properties, which in turn changes precipitation and the hydrological cycles [2]. On the other hand, anthropogenic emissions in urban/industrial regions, as well as the transport of dust storms and biomass burning smoke, have been proven to be very harmful to public health [3]. However, aerosols have very inhomogeneous distributions due to their short lifetime and diverse emission sources. To accurately study the climate and environmental effects of aerosols requires continuous observations on regional to global scales.

With the unique advantage of timely global coverage, dedicated satellite instruments have been launched continuously to obtain aerosol information since the late 1990s [4]. To accurately retrieve aerosol optical/microphysical parameters from satellite measurements is quite challenging due to the coupled atmosphere-surface signals [5]. As a result, various satellite instruments and retrieval algorithms have been developed to meet the requirements of certain aerosol parameters and calculation time. For instance, aerosol optical depth (AOD) is the only quantitative retrieval parameter from the multispectral measurements of Moderate Resolution Imaging Spectroradiometer (MODIS) using known aerosol scattering properties in pre-calculated lookup tables (LUTs). Owing to near-daily global coverage and high spatial resolution at 1–10 km, MODIS AOD derived from several operational algorithms has been the most widely used satellite aerosol parameter [6]. On the other hand, optimized inversions from multiangle polarimetric (MAP) observations of POLarization and Directionality of the Earth's Reflectances (POLDER) can retrieve a number of aerosol optical/microphysical parameters [7]. However, the optimized inversions are usually time-consuming and suffer from uncertainties of retrieved parameters with low information content in the iterative radiative transfer (RT) calculations.

By employing nine same multispectral cameras, Multi-angle Imaging SpectroRadiometer (MISR) onboard Terra satellite since 2000 provides a continuous and stable measurement of

aerosols, clouds, and surfaces from multiple viewing angles for more than 20 years [8]. Despite a lack of polarimetric measurements compared with future multiangle instruments such as multiangle imager for aerosols (MAIA) [9], MISR with a wide range of scattering angles provides a valuable testbed to explore the sensitivity of multiangle satellite measurements to size, absorption, and shape of different aerosol types [10]. Unlike optimized inversion of MAP measurements, MISR retrieves aerosol microphysical parameters from 74 aerosol mixtures predefined in LUT [11]. Despite a well global performance, the current MISR Version (V) 23 AOD tends to have a considerable underestimation in high values with also large uncertainties in aerosol microphysical parameters [12], [13]. With refined LUT and MODIS surface products, the accuracy of MISR aerosol retrievals exhibits notable improvement [14]. Besides LUT-based algorithms with discrete aerosol mixtures, how MISR retrievals can be improved by considering continuous aerosol properties has been rarely concerned.

Owing to a powerful ability to model the nonlinear relationship from multidimensional data, deep learning (DL) methods have been increasingly used in satellite remote sensing of atmospheric components [15]. By training the function relationship between satellite spectral reflectance at the top of atmosphere (TOA) and AErosol RObotic NETwork (AERONET) AOD and fine mode fraction, satellite retrievals with DL methods have obtained a higher accuracy than the common LUT algorithms in regional scales [16]. To overcome the dependence on ground measurements, RT simulations of satellite TOA reflectance and AOD are trained by DL methods [17]. Furthermore, recent exploratory studies show that DL methods can well establish the complex relationship between airborne multiangle observations and aerosol microphysical parameters based on their RT simulations [18], [19]. With high computational efficiency, the fast and flexible DL methods have great potential to improve retrievals of aerosol optical/microphysical properties from MISR measurement.

In this study, we present a flexible and robust retrieval algorithm for aerosol optical/microphysical properties from MISR measurements by combining atmospheric RT model and DL methods. Section II introduces MISR and AERONET measurements and their respective products. Then, Section III briefly describes the general framework of our MISR retrieval algorithm. The retrieval results and performance of our algorithm are analyzed by ground validation and inter-comparison with MISR products in Section IV. Section V gives a summary of the primary findings and conclusions.

II. SATELLITE AND GROUND MEASUREMENTS

A. MISR Measurements and Aerosol Products

The MISR instrument aboard the NASA Earth Observing System Terra satellite since December 1999 has a descending polar orbit with an equatorial crossing time of 10:30 local time. By employing nine identical cameras that have four bands centered at 446, 558, 672, and 866 nm, MISR measures spectral reflectance of the Earth's surface from the nadir and $\pm 26.1°$, $\pm 45.6°$, $\pm 60.0°$, and $\pm 70.5°$ forward or backward in the direction of the satellite flight track. MISR's nine

near-simultaneous observations cover a broad range of scattering angles between $\sim 60°$ and $160°$ at mid-latitudes. Besides a swath width of ~ 380 km, MISR's spectral measurements at nine viewing angles are calibrated and averaged into a uniform resolution of 1.1-km (https://misr.jpl.nasa.gov/Mission/).

The recent V23 MISR algorithm over land infers aerosol optical/microphysical properties over land by utilizing 74 predefined aerosol mixtures at a spatial resolution of 4.4 km [11]. Each of the 74 mixtures is composed of two or three aerosol components with different shapes, single scattering albedo (SSA), and particle sizes. Particle shapes include spherical, nonspherical grains and spheroids. SSA values of 0.80, 0.90, 0.98, and 1.0 at 558 nm are used to indicate strongly absorbing, moderately, weakly absorbing, and nonabsorbing aerosols. For particle size, the total AOD is assumed to be composed of small, medium, and large size bins with particle radius <0.35, 0.35–0.7, and >0.7 μm, respectively [20]. By searching for the best match between MISR spectral reflectance at TOA and their simulations calculated with 74 mixtures in the LUT, MISR retrievals will obtain an AOD value at a certain mixture passing the criteria. Once an aerosol mixture is selected in MISR retrieval, the aerosol component and size mode fraction AOD as well as corresponding SSA can be determined. Despite great improvement in retrieval accuracy of MISR AOD [12], the current V23 MISR AOD has systematic underestimation in polluted regions such as East Asia [13]. Here, we utilize V23 MISR products for inter-comparison with our retrieval.

B. AERONET Products

As a global ground-based remote sensing network of Sun photometers established since the 1990s, AERONET provides continuous and long-term well-calibrated measurements and inversion products of aerosol optical/microphysical parameters [21]. By measuring direct sunlight, AERONET spectral AODs at 440, 675, 870, and 1020 nm are calculated every 5–15 min at very high accuracy (~ 0.01–0.02), which are usually used as truth in the validation of satellite retrievals. Combined with directional measurements of the skylight at almucantar and MODIS bidirectional reflectance distribution function (BRDF), AERONET inversions include volume size concentration at 22 nodes, spectral complex refractive index, and nonsphericity. Thresholds of $AOD_{440 \text{ nm}} > 0.4$ and solar zenith angle (SZA) $>50°$ are used to make quality control of Level (L) 2.0 AERONET complex refractive index for almucantar measurements, and the scope of SZA is expanded to $>25°$ for hybrid measurements [22]. The AERONET inversions assume the same complex refractive index for both fine and coarse particles, which can be different from actual conditions. Here, we retrieve the spectral complex refractive index, effective radius (r_{eff}), and its effective variance (v_{eff}) of fine and coarse particles separately with the method by Xu et al. [23]. The Version 3 AERONET L2.0 or 1.5 products are only selected to validate our retrievals. Consistent with previous studies [12], a spatial window of 25 km diameter centered by the AERONET site and a temporal window of ± 30 min (1 hour for SSA) around satellite passing time are
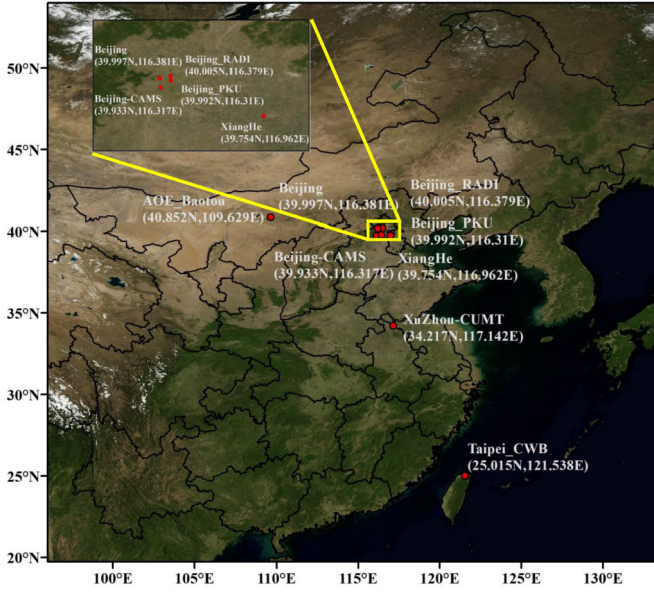
Fig. 1. Geographic location of AERONET sites (red) in MODIS true-color image of eastern China.

utilized to obtain matched MISR and AERONET observations. Fig. 1 shows the locations of the eight AERONET sites used in this study.

III. MISR Aerosol Retrieval With PDL Method

The common optimized methods make iterative RT calculations of all the retrieved aerosol and surface parameters together, in which unknowns with low information content can propagate retrieval errors. Moreover, iterative RT calculations have to be conducted in each retrieved pixel. The atmospheric RT model with reliable inputs gives a clear physical constraint between simulated satellite measurements and corresponding aerosol/surface parameters at various observation geometries. On the other hand, the DL methods have a marked advantage in modeling the high-order relationship between satellite measurements and retrieved aerosol optical/microphysical parameters. By combining RT simulations and the DL methods, we developed a physics-informed DL (PDL) aerosol retrieval algorithm for MISR (Fig. 2). Based on the full physical constraint in RT simulations, each interested aerosol/surface parameter can be modeled with the whole MISR measurements separately by the DL method.

A. Atmospheric RT Model

To generate the DL training datasets, the UNified and linearized vector RT model (UNL-VRTM) is utilized to simulate MISR measurements at various atmospheric and surface conditions. As a numerical testbed for aerosol remote sensing [24], UNL-VRTM mainly consists of a linearized vector RT model (VLIDORT), Rayleigh scattering and gas absorption module, aerosol scattering module, and surface bidirectional reflectance model (BRDF/BPDF).

UNL-VRTM supports up to two aerosol size modes, with their respective optical (AOD or volume concentration) and

microphysical properties (size distribution and complex refractive index) that can be configured separately and flexibly. Here, aerosols are assumed to be a mixture of two components: spherical fine particles and nonspherical coarse particles. The scattering parameters of nonspherical aerosols are calculated by the spheroid model from [25]. Particle sizes of both aerosol modes follow a bi-modal lognormal distribution:

$$\frac{dV}{d\ln r} = \sum_{i=1}^{2} \frac{V_0^i}{\sqrt{2\pi} \ln \sigma_g^i} \exp\left[-\frac{(\ln r - \ln r_v^i)^2}{2 \ln^2 \sigma_g^i}\right] \quad (1)$$

where V_0, r_v, and σ_g denote the total volume concentration ($\mu m^3 \mu m^{-2}$), geometric volume median radius, and geometric standard deviation, respectively. The particle size of fine and coarse mode ranges from 0.01 to 10 μm and 0.05 to 20 μm. The effective radius r_{eff} and effective variance v_{eff} are defined as

$$r_{eff} = r_v \exp\left(-\frac{1}{2}\ln^2\sigma_g\right) \quad (2)$$

$$v_{eff} = \exp\left(\ln^2\sigma_g\right) - 1. \quad (3)$$

The extinction efficiency factor, Q_{ext}, is the ratio of extinction and geometric cross section. The spectral AOD (τ_a, λ) can be calculated as

$$\tau_a(\lambda) = \sum_{i=1}^{2} \frac{3V_0^i Q_{ext}^i(\lambda)}{4r_{eff}^i}. \quad (4)$$

For surface BRDF, we select a widely used semi-empirical model that relies on a linear weighted sum of isotropic scattering, ross-thick volume scattering (K_{vol}), and li-sparse geometric scattering (K_{geo}) [26]

$$R(\lambda, \vartheta_0, \vartheta_v, \varphi) = f_{iso}(\lambda) + f_{vol}(\lambda)K_{vol}(\vartheta_0, \vartheta_v, \varphi) \\ + f_{geo}(\lambda)K_{geo}(\vartheta_0, \vartheta_v, \varphi) \quad (5)$$

where f_{iso}, f_{vol}, and f_{geo} are spectral-dependent weighting parameters. Here, ϑ_0, ϑ_v, and φ are solar zenith, view zenith, and relative azimuth angles, respectively.

B. Deep Belief Network

The deep belief network (DBN) is a probabilistic generative model composed of stacked restricted Boltzmann machines (RBM) and an error backpropagation (BP) net. The DBN includes an unsupervised pretraining of RBM and supervised fine-tuning by BP [27]. RBM is used to detect patterns and inherent information of the training dataset by learning its probabilistic distribution. As an undirected and generative energy-based model, RBM has a visible input layer and a hidden feature-extracting layer with connections between but not within layers. With the hidden layer serving as the visible layer for the next RBM, DBN has a fast greedy layer-by-layer training process with the contrastive divergence method. After the unsupervised training, error backpropagation algorithms are utilized to fine-tune the weights of each RBM connection in reverse to get optimal performance for generating the training datasets. As an efficient and robust learning model, DBN has good generalization and anti-noise abilities and can even learn features from the raw data. Thus, we select DBN to make aerosol retrieval in this study.
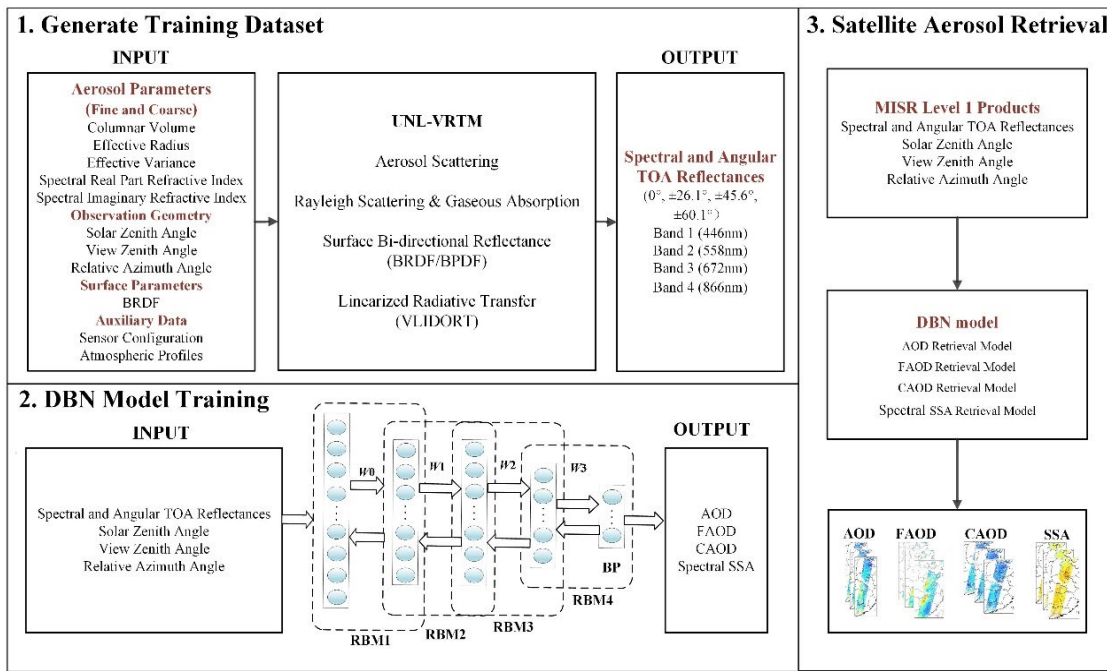
Fig. 2.   Flowchart of PDL aerosol algorithm for multiangle MISR measurements.

C. MISR PDL Aerosol Algorithm

As shown in Fig. 2, the MISR PDL algorithm comprises three key modules. The first module generates training datasets by RT simulation using UNL-VRTM. Based on the full physical constraint among simulated satellite measurement, aerosols, and surface, retrieved aerosol parameters are modeled with the whole used MISR measurements separately with the DBN method in the second module. Then, aerosol retrieval from the real MISR data is implemented with trained DBN models.

1) To generate training datasets for MISR retrievals, the spectral and angular MISR TOA reflectance is simulated by UNL-VRTM. Instead of inputting random combinations of aerosol/surface parameters and satellite observation geometries, we make full use of the abundant prior information from existing ground measurements and satellite products. For aerosol optical/microphysical parameters, we utilize our own inversions of aerosol microphysical parameters for fine and coarse mode separately from continuous sun photometer measurements in the AERONET site of Beijing during 2015–2021 with the optimized method by Xu et al. [23]. There are a total number of 2605 aerosol inversions from the seven-year ground measurements in Beijing, which is influenced by local urban/industrial emissions, long-range transport of dust particles, and fire smoke, as well as their mixtures.

Then, MODIS BRDF product in eastern China during 2017 with collocated MISR observation geometry and altitudes are combined randomly with each inversion of aerosol optical/microphysical parameters in the Beijing site. For aerosol profiles, a fixed Gaussian distribution within 3 km and peak height at 1.5 km is assumed. In addition, mid-latitude summer and mid-latitude winter atmospheric profiles are used.

Comparison with single-pixel MISR measurements shows that UNL-VRTM simulations have a robust and reliable performance (Fig. 3). Simulated MISR spectral reflectance at 446, 558, and 672 nm are very closely concentrated along the 1:1 line with MISR measurement for view zenith angles (VZAs) $\leq 60.1°$ with high correlation coefficient (R: 0.90–0.978) and low root-mean-square error (RMSE: 0.01–0.018). Simulated MISR TOA reflectance at near-infrared band of 866 nm gets slightly scattered, which is more sensitive to changes in surface types. However, simulated MISR TOA reflectance exhibits obvious systematic underestimation at large VZA of $\pm 70.5°$. Therefore, we only utilize RT simulations at seven MISR viewing angles of $0°$, $\pm 26.1°$, $\pm 45.6°$, and $\pm 60.1°$ for training.

2) Module 2 takes the simulated MISR measurements as input and aerosol parameters as output to train their function relationships with DBN. Since there are too many unknowns for aerosol optical/microphysical parameters, we converted them into AOD, fine AOD (FAOD), coarse AOD (CAOD) at 550 nm, and spectral SSA before training. Then, the simulated seven angular MISR measurements are modeled with these aerosol parameters separately. A random 20% of the training dataset is not used for training but for testing the trained models, in which simulations are the input for retrieval, and aerosol datasets are "true values" for validation. Fig. 4 shows the validation of PDL retrievals using the 20% test dataset. The PDL AOD and FAOD have high accuracy with $R > 0.99$ and RMSE ≤ 0.063. Although PDL CAOD values get scattered, nearly 90% of the retrievals are within the expected error (EE) envelope of $(0.05 \pm 20\%\text{AOD})$. Despite the obvious bias, PDL SSA exhibits very consistent variations with true values and is concentrated along a 1:1 line with R around 0.69–0.76.

3) With these trained DBN models, aerosol retrieval from the selected seven angular MISR measurements is implemented over eastern China during 2015–2019.
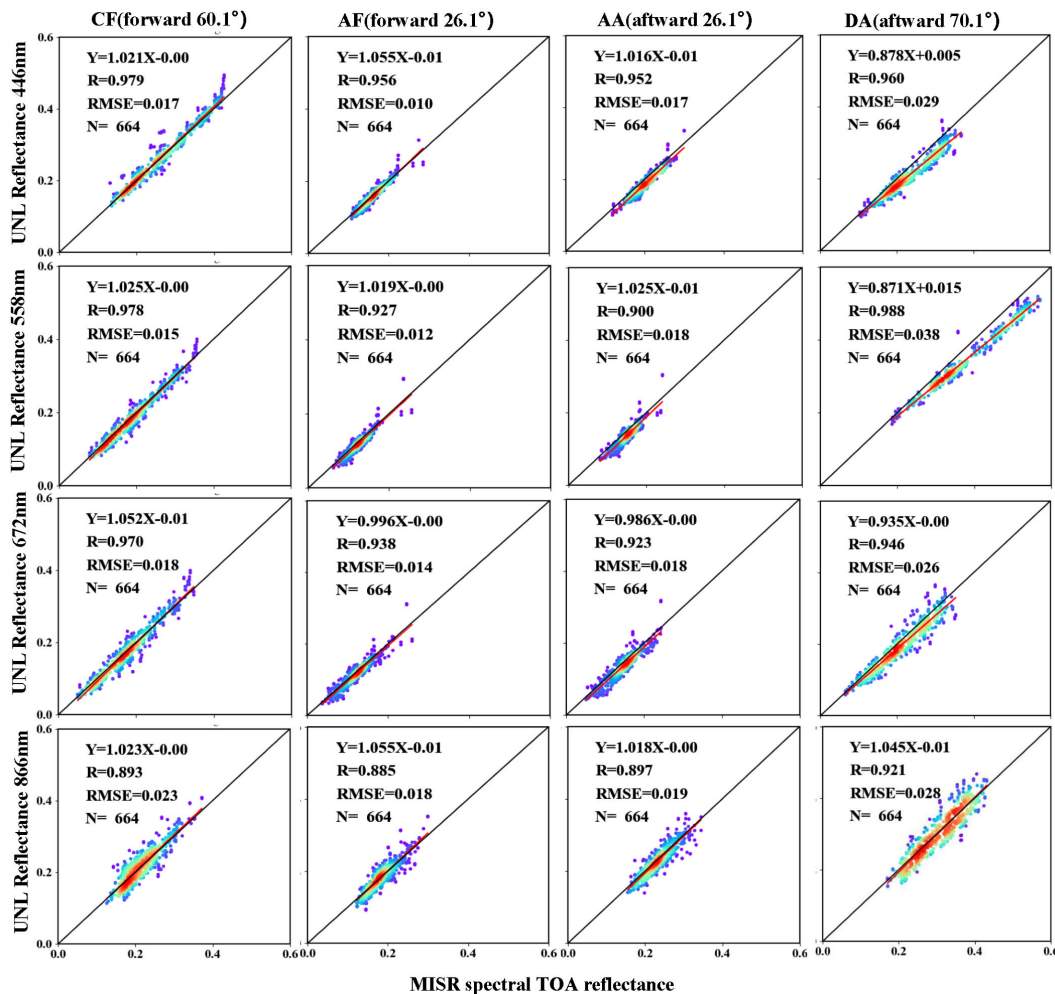
Fig. 3. Comparison of RT simulations with corresponding single-pixel MISR TOA spectral reflectance.

IV. RESULTS AND ANALYSIS

A. Validation of PDL Aerosol Retrievals From MISR Measurements

Fig. 5 shows the ground-based validation of MISR V23 standard aerosol (SA) retrieval and PDL results using AERONET products in eastern China during 2015–2019. Both MISR V23 and PDL AOD exhibit high accuracy with more than 85% retrieval values within the EE envelope of ± (0.05 + 20%). MISR PDL has a higher correlation coefficient ($R = 0.974$) and lower RMSE ($= 0.095$) than V23 ($R = 0.943$ and RMSE $= 0.181$). In particular, PDL retrievals avoid the underestimation problem of V23 MISR AOD at high values (>0.5).

While there is an obvious decrease in retrieval accuracy of V23 MISR FAOD ($R = 0.844$ and RMSE $= 0.234$), PDL FAOD has a very close accuracy ($R = 0.958$ and RMSE $= 0.103$) with PDL AOD. It should be stated that MISR V23 FAOD includes the contribution from both small model aerosol with radius <0.35 μm and medium mode within 0.35–0.70 μm. Moreover, MISR V23 FAOD exhibits a much larger underestimation in high values (>0.5), which can be the main error source of the total AOD.

Despite more than 75% of both MISR V23 and PDL CAOD values within the EE, their retrievals get very scattered compared with AERONET products with notable abnormal values (Fig. 5). Since fine particles are predominant in eastern China, most CAOD values are below 0.2, at which the information content of coarse particles is limited [28]. PDL CAOD has a higher correlation ($R = 0.588$) with AERONET products than V23 retrieval ($R = 0.354$) with relatively fewer abnormal values. However, large overestimation exists in some low values of PDL CAOD.

Compared with the large overestimation of MISR V23 SSA, PDL retrievals exhibit a great improvement in correlation and consistency with AERONET inversion (Fig. 6). The performance of PDL SSA has a marked dependence on wavelength, with much higher accuracy for longer bands at 672 and 866 nm, which can reflect variations of aerosol absorption reliably. PDL SSA at 672 nm has a slightly higher correlation and lower RMSE and gets scattered at 866 nm. By contrast, the sensitivity of PDL retrieval to SSA at 472 nm is obviously lower, with overestimation for SSA <0.9 and underestimation for SSA >0.9. The predominant contribution from Rayleigh scattering at large VZAs can be the main cause.
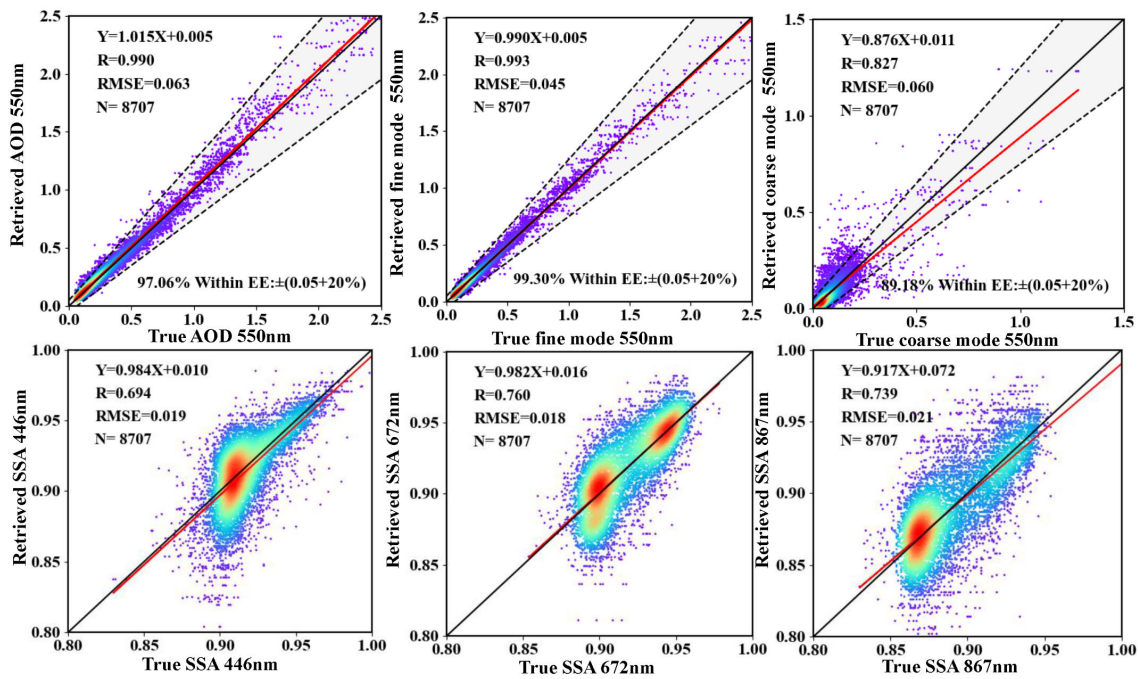
Fig. 4. Comparison of PDL retrievals using RT simulations and true AOD, FAOD, and CAOD at 550 nm, and SSA at 446, 672, and 866 nm values from the test data. The black and dashed lines are EE of ± (0.05% + 20%) and 1:1 line. Correlation coefficient (R), RMSE, and number (N) of retrieved-truth matchups are also shown.
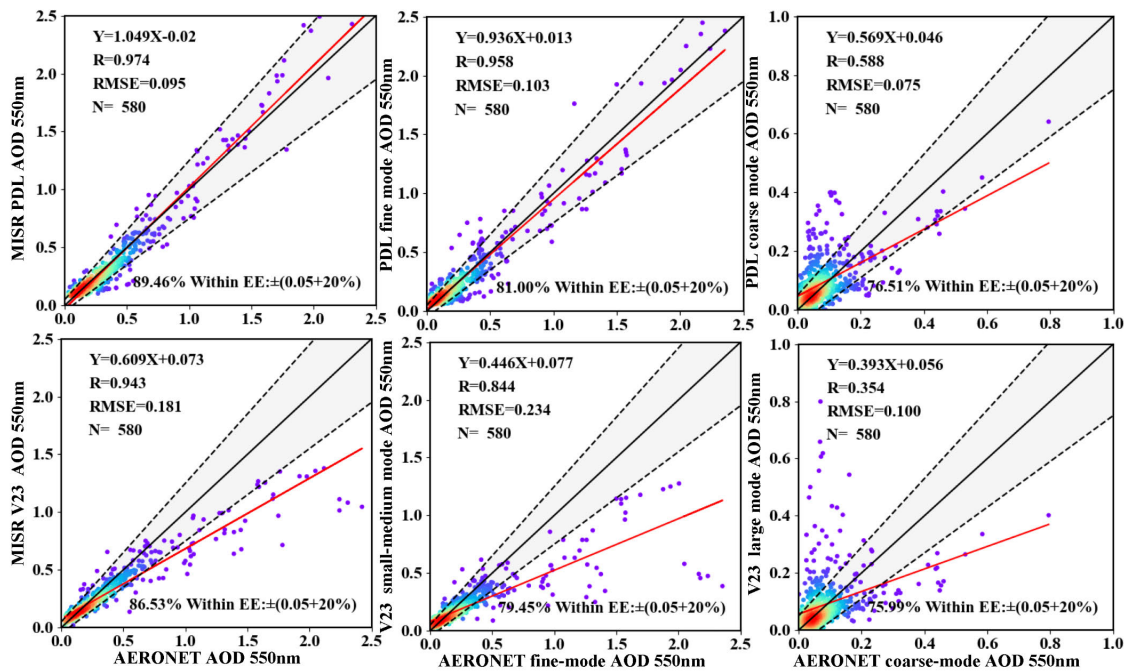

Fig. 5. Ground-based validation of MISR PDL and MISR V23 AOD, FAOD, and CAOD at 550 nm with AERONET products. The black and dashed lines are EE of ± (0.05% + 20%) and 1:1 line.

Generally, the MISR PDL algorithm implements a reliable and robust retrieval of aerosol optical/microphysical properties by making full use of the multiangle measurement and prior information of existing MODIS BRDF and AERONET aerosol inversions. Even only seven angular measurements are utilized, and MISR PDL retrievals have an obviously higher accuracy than LUT-based V23 MISR products. Moreover, the MISR PDL algorithm has very high computational efficiency, and

aerosol retrieval of one image in eastern China only takes several seconds for a common personal computer.

B. Inter-Comparison of MISR PDL and V23 Retrievals

Fig. 7 shows the annual mean of collocated MISR PDL and V23 retrievals over eastern China during 2017. Despite consistent spatial distribution, the magnitude of PDL and
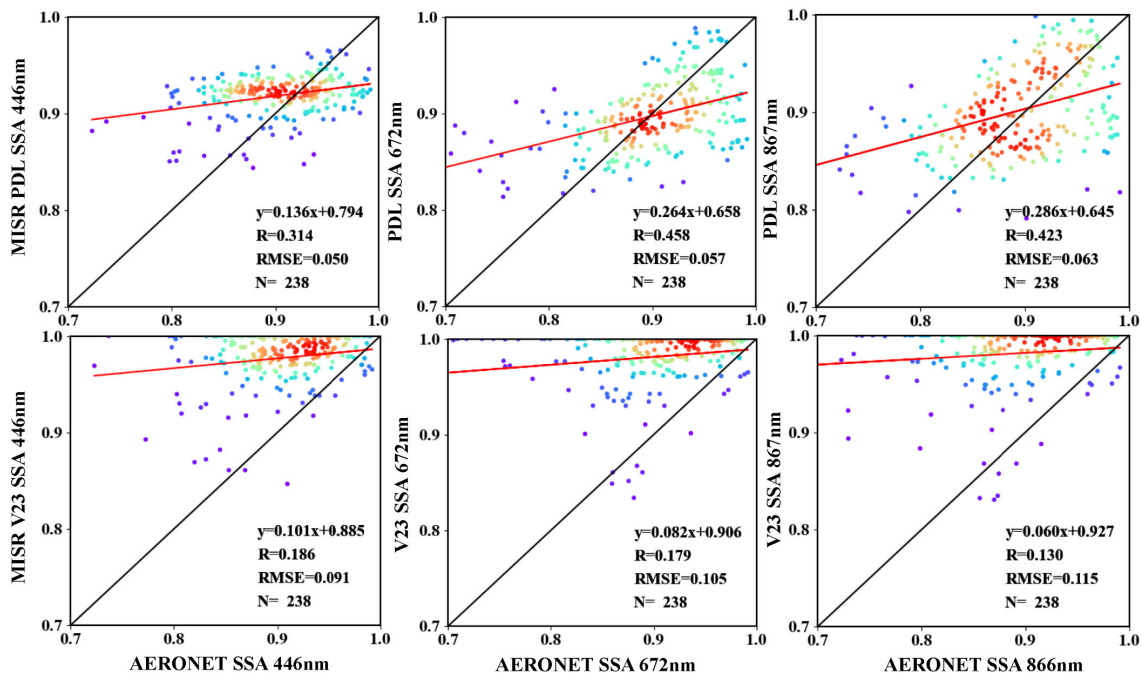
Fig. 6. Scatter plots of MISR SSA and AERONET inversions at 446, 672, and 866 nm for (top) PDL and (bottom) MISR V23 algorithms. The black and red lines denote 1:1 and linear fitting lines, respectively.

V23 retrievals exhibits distinct variations. Compared with V23 MISR AOD, PDL retrievals are much higher for moderate-to-high values (>0.4) in polluted regions. The large overestimation of MISR V23 SSA can be the main cause of systematic underestimation in AOD [13]. MISR PDL FAOD clearly reveals anthropogenic emission hotspots in urban/industrial regions of eastern China. MISR V23 CAOD exhibits notable high values (>0.3) in the south of eastern China, where fine particles are predominant. By contrast, PDL retrievals have a better spatial self-consistence with few high CAOD values in eastern China and more high values in the northwestern Gobi deserts.

To further examine the performance of MISR PDL retrieval, a typical dust event on May 4, 2017 is analyzed (Fig. 8). Consistent with comparison of the annual mean (Fig. 7), the distinct difference between daily MISR PDL and V23 AOD mainly exists in polluted regions. While dust plumes are concentrated over northern China, MISR PDL CAOD can well capture the prevailing dust particles after dust transport. Though not obviously, MISR PDL SSA gets slightly lower from west to east as the dust particles mixed with anthropogenic emissions in northern China.

Moreover, we inspected MISR PDL and V23 retrievals in a biomass burning event on June 13, 2012 (Fig. 9) when widespread fire emissions were blown northerly [29]. MISR PDL AOD and FAOD can clearly give the spatial distribution of the dense fire smoke. MISR PDL SSA at 672 nm over the agricultural fires is obviously lower (~0.90) than their downwind regions in the north (~0.95), indicating a prominent sensitivity to absorbing aerosols. The fresh fire smoke can get aged and mix with local anthropogenic emissions in the transport.

As shown in ground-based validation and inter-comparison, the MISR PDL algorithm can provide a reliable and robust retrieval of aerosol optical/microphysical parameters over eastern China. MISR PDL retrievals not only avoid the systematic underestimation in MISR V23 AOD at moderate-to-high values (>0.4) but also significantly improve the accuracy of FAOD and CAOD and spectral SSA. With the high computational efficiency of LUT-based retrieval, the MISR PDL algorithm exhibits great potential in the operational retrieval of aerosol/surface properties. In particular, the reliable performance of MISR PDL retrievals demonstrates that it is crucial to make a large range of scattering angles in future satellite instruments for aerosol observation.

C. Uncertainty and Implication of the MISR PDL Algorithm

Considering the notable bias of our RT simulation at the large VZA of 70.5° (Fig. 3), MISR PDL retrieval only utilizes seven angular measurements within 60.1°, which does not fully make use of the MISR observations. The increased uncertainties in the Ross-Thick/Li-Sparse BRDF model at large VZAs (≥70°) can be the main cause of simulation errors [30]. Though RT simulations and spectral MISR TOA measurements are very closely concentrated along the 1:1 line with high correlation, simulated MISR reflectance such as at 866 nm is a little scattered with an RMSE of ~0.02 that can lead to considerable bias in physically optimized inversion. Fortunately, the DBN method makes learning of probabilistic distribution of the whole training dataset rather than depending on absolute physical quantities. Therefore, DBN training has striking generalization ability and the advantage of anti-noise, which is robust to uncertainties
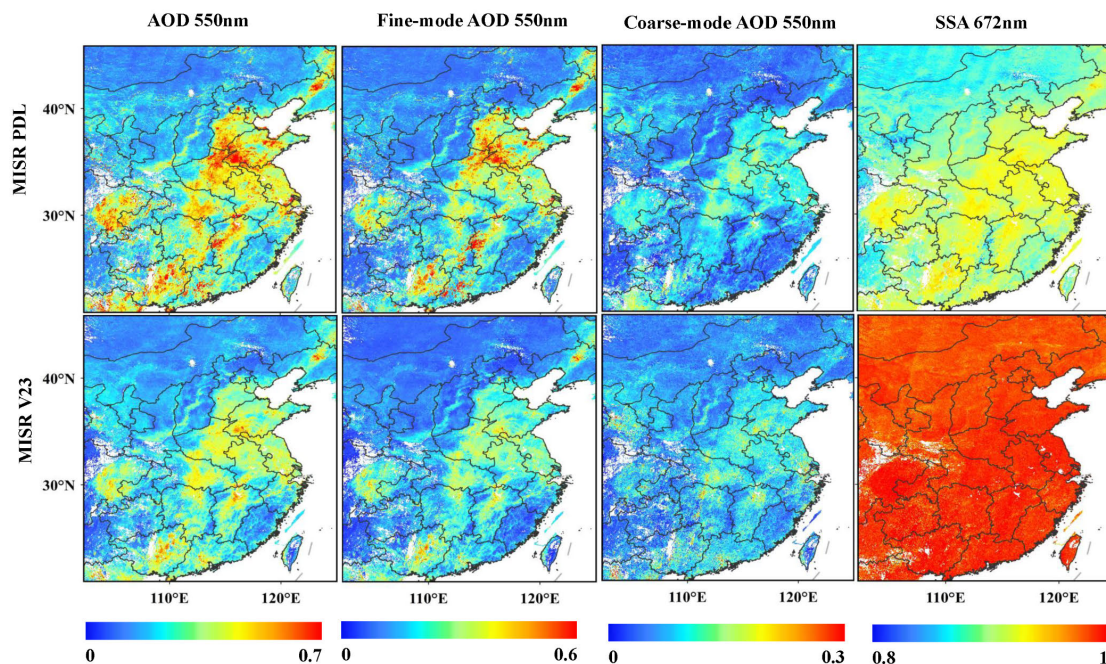
Fig. 7. Annual mean of MISR AOD, FAOD, and CAOD at 550 nm, and SSA at 670 nm for PDL and MISR V23 algorithm in eastern China during 2017.
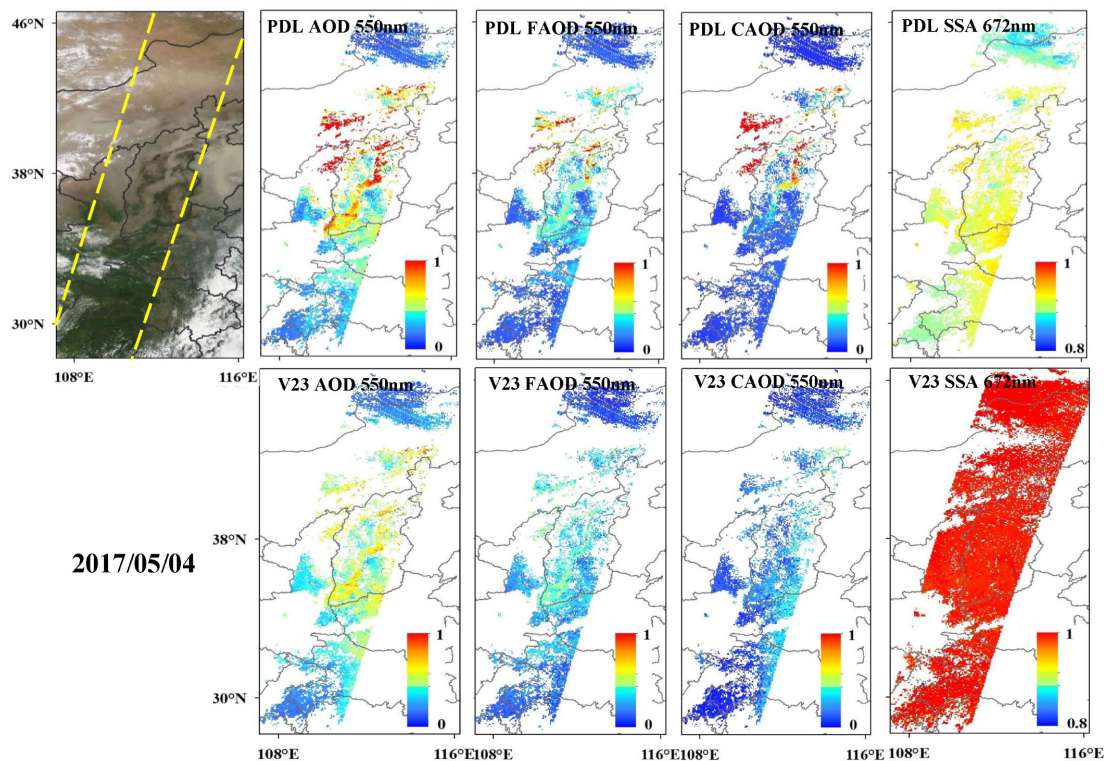

Fig. 8. MISR AOD, FAOD, and CAOD at 550 nm, and SSA at 672 nm for (top) PDL and (bottom) MISR V23 algorithm in northern China on May 4, 2017.

of RT simulations as well as radiometric noise of satellite instruments.

Despite a high accuracy for AOD and FAOD, MISR PDL CAOD and spectral SSA remain subject to considerable bias due to their limited information content in MISR measurements (Figs. 5 and 6). For optimized inversion of POLDER aerosol products, the generalized retrieval of aerosol and surface properties (GRASPs) models algorithm assumes that aerosols are composed of several known aerosol types with fixed complex refractive index, size distribution, and nonsphericity and retrieves their respective concentrations [8]. With the prior constraint for aerosol microphysical properties, POLDER AOD from GRASP/models has higher accuracy than that of GRASP optimized directly retrieving all aerosol
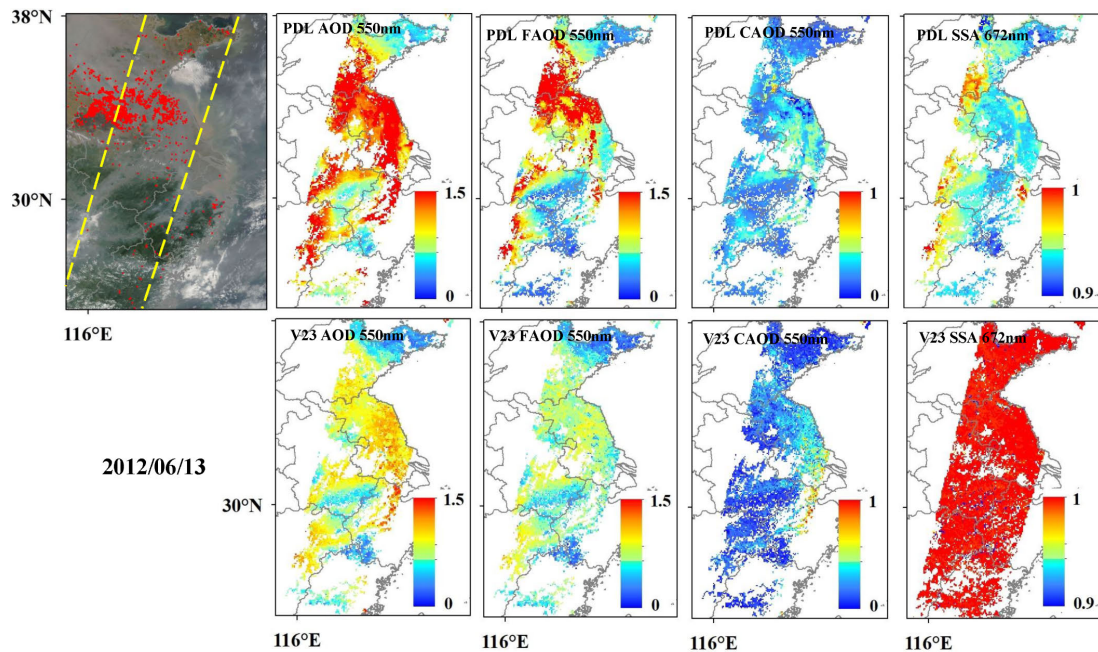
Fig. 9. MISR AOD, FAOD, and CAOD at 550 nm, and SSA at 672 nm for (top) PDL and (bottom) MISR V23 algorithm in China on June 13, 2012.

optical/microphysical parameters. It should be stated that the fixed aerosol models in LUTs of MODIS and MISR algorithms are also effective prior information derived from AERONET observations. Compared with the limited aerosol models or their mixtures in MODIS and MISR LUTs, GRASP/models make optimized retrieval of respective concentration of distinct aerosol types derived from global AERONET observations in a continuous space [8]. Similar prior constraints can be utilized flexibly in PDL retrieval to improve aerosol parameters with low information content or expand PDL to larger regions or global scale. In addition, the fixed aerosol profile used in PDL can increase retrieval bias for very high aerosol layers (e.g., >5 km).

The MISR PDL algorithm provides a flexible and robust framework for making full use of both satellite measurement and existing prior information. With the physical constraint in RT simulations, satellite measurements can be modeled with each aerosol unknown separately, which not only avoids error propagation in iterative RT calculations of optimized inversion but also ensures an efficient use of observational information. On the other hand, ground-based aerosol inversions and satellite BRDF can be flexibly utilized as prior information, enabling effective constraints and training. The future MAP satellite instruments such as MAIA have greatly expanded spectral range and polarimetric measurements, exerting a higher requirement on the efficiency of aerosol retrieval. With striking computational efficiency, reliable performance, and a flexible framework, the PDL algorithm has a prominent potential for operational aerosol retrieval of future MAP measurements with explosive growth in data volume.

V. CONCLUSION

Since the information content of satellite measurements is usually limited in inferring all aerosol/surface unknowns, how to accurately and efficiently retrieve as many aerosol param-

eters as possible has been a challenging problem in satellite retrieval. Despite a lack of polarization, MISR measurement at a large range of scattering angles is sensitive to aerosol microphysical properties. The current LUT-based MISR V23 products provide global aerosol microphysical parameters with a good self-consistent performance but have considerable uncertainties in regional scales such as eastern China. Based on a PDL method, we improve MISR aerosol retrievals over land by making efficient use of multiangle measurements and priori information from existing aerosol inversions and satellite BRDF products. Though only seven MISR angular measurements ($\pm70.5°$ not used) are utilized, the PDL algorithm has gained significant improvements compared with MISR V23 products. Moreover, the combination of physical constraints in RT simulation and DBN modeling enables each aerosol unknown to be modeled with the seven angular MISR measurements separately, which avoids error propagation in the optimized inversion. The PDL algorithm with reliable and robust performance as well as high computational efficiency exhibits great application potential in the operational retrieval of aerosol optical/microphysical parameters from multiangle or MAP satellite measurements.

REFERENCES

[1] I. Koren, Y. J. Kaufman, L. A. Remer, and J. V. Martins, "Measurement of the effect of Amazon smoke on inhibition of cloud formation," *Science*, vol. 303, no. 5662, pp. 1342–1345, Feb. 2004.

[2] Y. J. Kaufman, D. Tanré, and O. Boucher, "A satellite view of aerosols in the climate system," *Nature*, vol. 419, no. 6903, pp. 215–223, Sep. 2002.

[3] C. A. Pope III et al., "Lung cancer, cardiopulmonary mortality, and long-term exposure to fine particulate air pollution," *J. Amer. Med. Assoc.*, vol. 287, no. 9, pp. 1132–1141, 2002.

[4] M. D. King, Y. J. Kaufman, D. Tanré, and T. Nakajima, "Remote sensing of tropospheric aerosols from space: Past, present, and future," *Bull. Amer. Meteorol. Soc.*, vol. 80, pp. 2229–2260, Jul. 1999.

[5] O. Dubovik et al., "Polarimetric remote sensing of atmospheric aerosols: Instruments, methodologies, results, and perspectives," *J. Quant. Spectrosc. Radiat. Transf.*, vol. 224, pp. 474–511, Feb. 2019.

[6] R. C. Levy et al., "The collection 6 MODIS aerosol products over land and ocean," *Atmos. Meas. Techn.*, vol. 6, no. 11, pp. 2989–3034, Nov. 2013.

[7] C. Chen et al., "Validation of GRASP algorithm product from POLDER/PARASOL data and assessment of multi-angular polarimetry potential for aerosol monitoring," *Earth Syst. Sci. Data*, vol. 12, no. 4, pp. 3573–3620, Dec. 2020.

[8] D. J. Diner et al., "The value of multiangle measurements for retrieving structurally and radiatively consistent properties of clouds, aerosols, and surfaces," *Remote Sens. Environ.*, vol. 97, no. 4, pp. 495–518, Sep. 2005.

[9] D. J. Diner et al., "Advances in multiangle satellite remote sensing of speciated airborne particulate matter and association with adverse health effects: From MISR to MAIA," *J. Appl. Remote Sens.*, vol. 12, no. 4, Jul. 2018, Art. no. 042603.

[10] R. A. Kahn and B. J. Gaitley, "An analysis of global aerosol type as retrieved by MISR," *J. Geophys. Res., Atmos.*, vol. 120, no. 9, pp. 4248–4281, May 2015.

[11] M. J. Garay et al., "Introducing the 4.4 km spatial resolution Multi-angle Imaging SpectroRadiometer (MISR) aerosol product," *Atmos. Meas. Techn.*, vol. 13, no. 2, pp. 593–628, Feb. 2020.

[12] M. J. Garay, O. V. Kalashnikova, and M. A. Bull, "Development and assessment of a higher-spatial-resolution (4.4 km) MISR aerosol optical depth product using AERONET-DRAGON data," *Atmos. Chem. Phys.*, vol. 17, no. 8, pp. 5095–5106, Apr. 2017.

[13] M. Tao et al., "Characterization of aerosol type over east Asia by 4.4 km MISR product: First insight and general performance," *J. Geophys. Research: Atmos.*, vol. 125, no. 13, Jul. 2020, Art. no. e2019JD031909.

[14] J. A. Limbacher, R. A. Kahn, and J. Lee, "The new MISR research aerosol retrieval algorithm: A multi-angle, multi-spectral, bounded-variable least squares retrieval of aerosol particle properties over both land and water," *Atmos. Meas. Techn.*, vol. 15, no. 22, pp. 6865–6887, Nov. 2022.

[15] X. Chen, J. Wang, J. Gomes, O. Dubovik, P. Yang, and M. Saito, "Analytical prediction of scattering properties of spheroidal dust particles with machine learning," *Geophys. Res. Lett.*, vol. 49, no. 9, p. 49, May 2022.

[16] Y. Kang, M. Kim, E. Kang, D. Cho, and J. Im, "Improved retrievals of aerosol optical depth and fine mode fraction from GOCI geostationary satellite data using machine learning over East Asia," *ISPRS J. Photogramm. Remote Sens.*, vol. 183, pp. 253–268, Jan. 2022.

[17] C. Jia, L. Sun, Y. Chen, Q. Liu, H. Yu, and W. Zhang, "Satellite aerosol retrieval using scene simulation and deep belief network," *IEEE Trans. Geosci. Remote Sens.*, vol. 60, pp. 1–16, 2022, Art. no. 4104516.

[18] A. Di Noia, O. P. Hasekamp, L. Wu, B. van Diedenhoven, B. Cairns, and J. E. Yorks, "Combined neural network/Phillips–Tikhonov approach to aerosol retrievals over land from the NASA research scanning polarimeter," *Atmos. Meas. Techn.*, vol. 10, no. 11, pp. 4235–4252, Nov. 2017.

[19] M. Gao et al., "Efficient multi-angle polarimetric inversion of aerosols and ocean color powered by a deep neural network forward model," *Atmos. Meas. Techn.*, vol. 14, no. 6, pp. 4083–4110, Jun. 2021.

[20] R. A. Kahn et al., "Multiangle imaging SpectroRadiometer global aerosol product assessment by comparison with the aerosol robotic network," *J. Geophys. Res., Atmos.*, vol. 115, no. D23, pp. 1–28, Dec. 2010.

[21] B. N. Holben et al., "AERONET—A federated instrument network and data archive for aerosol characterization," *Remote Sens. Environ.*, vol. 66, no. 1, pp. 1–16, Oct. 1998.

[22] D. M. Giles et al., "Advancements in the aerosol robotic network (AERONET) version 3 database-automated near-real-time quality control algorithm with improved cloud screening for sun photometer aerosol optical depth (AOD) measurements," *Atmos. Meas. Techn.*, vol. 12, no. 1, pp. 169–209, Jan. 2019.

[23] X. Xu et al., "Retrieval of aerosol microphysical properties from AERONET photopolarimetric measurements: 2. A new research algorithm and case demonstration," *J. Geophys. Res., Atmos.*, vol. 120, no. 14, pp. 7079–7098, 2015.

[24] J. Wang et al., "A numerical testbed for remote sensing of aerosols, and its demonstration for evaluating retrieval synergy from a geostationary satellite constellation of GEO-CAPE and GOES-R," *J. Quant. Spectrosc. Radiat. Transf.*, vol. 146, pp. 510–528, Oct. 2014.

[25] O. Dubovik et al., "Application of spheroid models to account for aerosol particle nonsphericity in remote sensing of desert dust," *J. Geophys. Res., Atmos.*, vol. 111, no. D11, pp. 1–34, Jun. 2006.

[26] W. Lucht, C. B. Schaaf, and A. H. Strahler, "An algorithm for the retrieval of albedo from space using semiempirical BRDF models," *IEEE Trans. Geosci. Remote Sens.*, vol. 38, no. 2, pp. 977–998, Mar. 2000.

[27] G. E. Hinton, S. Osindero, and Y.-W. Teh, "A fast learning algorithm for deep belief nets," *Neural Comput.*, vol. 18, no. 7, pp. 1527–1554, Jul. 2006.

[28] W. Dong et al., "Satellite aerosol retrieval from multiangle polarimetric measurements: Information content and uncertainty analysis," *IEEE Trans. Geosci. Remote Sens.*, vol. 61, pp. 1–13, 2023, Art. no. 4101813.

[29] M. Tao, L. Chen, Z. Wang, J. Tao, and L. Su, "Satellite observation of abnormal yellow haze clouds over East China during summer agricultural burning season," *Atmos. Environ.*, vol. 79, pp. 632–640, Nov. 2013.

[30] P. Litvinov, O. Hasekamp, and B. Cairns, "Models for surface reflection of radiance and polarized radiance: Comparison with airborne multiangle photopolarimetric measurements and implications for modeling top-of-atmosphere measurements," *Remote Sens. Environ.*, vol. 115, no. 2, pp. 781–792, Feb. 2011.

Wenjing Man received the M.S. degree from China University of Geosciences, Wuhan, China, in 2021, where she is currently pursuing the Ph.D. degree with the School of Geography and Information Engineering, with a focus on the research of satellite aerosol retrieval algorithms.

Minghui Tao received the Ph.D. degree from Chinese Academy of Sciences (CAS), Beijing, China, in 2013.

He was with the Institute of Remote Sensing and Digital Earth, CAS, from 2013 to 2017. He is currently a Professor with the School of Geography and Information Engineering, China University of Geosciences, Wuhan, China. His research interests include satellite remote sensing of atmospheric environment and their application in air quality and climate change.

Lina Xu received the Ph.D. degree from Chinese Academy of Sciences, Beijing, China, in 2007.

She is currently an Associate Professor with the School of Geophysics and Spatial Information, China University of Geosciences, Wuhan, China. Her main research interests include remote sensing image processing, remote sensing geology applications, and microwave remote sensing applications (surface parameter acquisition and surface deformation monitoring).
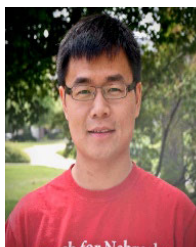
Xiaoguang Xu received the Ph.D. degree from the University of Nebraska–Lincoln, Lincoln, NE, USA, in 2015.

He is currently a Research Scientist with the University of Maryland, Baltimore County, Baltimore, MD, USA. He has developed aerosol algorithms for both satellite and ground-based remote sensing platforms. He is the primary developer of a numerical testbed for remote sensing of aerosol known as UNL-VRTM. His research area has focused on the development of retrieval algorithms and data assimilation of aerosol remote sensing data.

Yi Wang received the Ph.D. degree in geoinformatics from the University of Iowa, Iowa City, IA, USA, in 2019.

He is currently a Professor with the School of Geography and Information Engineering, China University of Geosciences, Wuhan, China. His research interests include satellite remote sensing of aerosols and assimilation of satellite data in inversion of pollution emission inventory.

Jianfang Jiang received the M.S. degree from Capital Normal University, Beijing, China, in 2021. She is currently pursuing the Ph.D. degree with the School of Geography and Information Engineering, China University of Geosciences, Wuhan, China, with a focus on the research of atmospheric environmental remote sensing inversion algorithms.

Meng Fan received the Ph.D. degree in cartography and geographic information system from the Institute of Remote Sensing and Digital Earth, Chinese Academy of Sciences, Beijing, China, in 2014.

She is currently an Associate Researcher with the Aerospace Information Research Institute, Chinese Academy of Sciences. Her research interests include remote sensing of atmospheric chemical components, aerosol scattering simulation, and satellite-based thermal anomaly detection.

Jun Wang (Member, IEEE) received the Ph.D. degree in atmospheric sciences from The University of Alabama in Huntsville, Huntsville, AL, USA, in 2005.

He is currently a Professor and the Chair of the Department of Chemical and Biochemical Engineering, University of Iowa, Iowa City, IA, USA. He is also a James E. Ashton Professorship of Engineering and the Assistant Director of Iowa Technology Institute, Iowa City. His research interests include satellite remote sensing of aerosols and fires, chemistry transport modeling, data assimilation, inverse optimization, and integration of these elements to study air quality and aerosol–cloud interaction.

Lunche Wang received the Ph.D. degree from Wuhan University, Wuhan, China, in 2015.

He is currently a Professor with the School of Geography and Information Engineering, China University of Geosciences, Wuhan. His research interests include climate change and remote sensing of environment.

Liangfu Chen received the Ph.D. degree in geography from the Institute of Remote Sensing and Geographical Information System, Peking University, Beijing, China, in 1999.

He is currently a Professor with the Aerospace Information Research Institute, Chinese Academy of Sciences, Beijing. His research interests include satellite retrieval of atmospheric aerosol and trace gases as well as their application in carbon neutrality.